



Cite this: *J. Mater. Chem. C*, 2021, 9, 4182

Combined effects of ion-pairing on multi-emissive properties of benzimidazolium salts†

Gabriele Di Carlo,^a Alessandra Forni,^b Paola Moretti,^a Daniele Marinotto,^b Chiara Botta,^c Maddalena Pizzotti,^a Francesca Tessore^a and Elena Cariati^a

The possibility to control luminescence properties of purely organic emitting salts is receiving an ever-growing interest. A full understanding of the manifold effects of counterions on the photophysical properties of charged luminophors deserves thorough investigation. Here, we disclose the impact of different anions, *i.e.* triflate, iodide and nitrate, on the multiple emissions of a new class of ionic luminophors, based on 1,3-dimethyl-2-(*p*-tolyl)-1*H*-benzo[*d*]imidazol-3-ium, **1**. The specific ion-pairing plays a key role in the emissive properties of solids, depending on both the electronegativity of the anion and its distance from the cation. Three main effects emerge from strong ion-pairing: (i) fluorescence quenching, (ii) phosphorescence enhancement and (iii) efficient direct population of the triplet-state. As a result, a weak interaction (**1-OTf**) guarantees intense fluorescence (QY > 50%), while a strong pairing (**1-NO₃·0.5EtOH** and **1-I·0.5CH₂Cl₂**) promotes molecular room temperature phosphorescence (RTP) enhancement. The anion-controlling strategy also enables long-lasting RTP (288 ms) in **1-OTf** and ultrabright phosphorescence (QY > 70%) in **1-NO₃·0.5EtOH**, under direct triplet-excitation at 350 nm.

Received 1st February 2021,
Accepted 26th February 2021

DOI: 10.1039/d1tc00503k

rsc.li/materials-c

Introduction

To date purely organic compounds exhibiting room temperature luminescence in the solid state have made impressive strides as advanced optical materials for a wide range of potential applications.^{1–3} The profitable properties, such as low-cost starting materials, rationally tailored molecular structures and good processability under mild conditions, make them very attractive.^{4–7} Molecular design,^{2,8,9} crystal packing engineering,^{10,11} co-crystallization¹² and heavy atom effect^{13,14} are some viable strategies explored in the last decade to boost the phosphorescence of light-emitting solids. The switch between fluorescence and phosphorescence emissions has also been precisely regulated either through external stimuli, such as mechanical forces and pH variation,^{15,16} or molecular design.¹⁷

Very recently, a growing interest has emerged in designing organic salts as solid emitters with tunable photophysical properties by varying both cation¹⁸ and anion constituents.^{6–9}

Variation of halides, as counterions, has been explored as a viable strategy to manipulate the photophysical properties of cationic emitters.^{19,20} On one hand, the counter-ion of light-emitting salts may positively affect their crystal packing,²¹ resulting in enhanced emissive properties by reducing non-radiative decay channels.²² On the other hand, electronic coupling within ionic pairs is expected to influence the compound's photophysical properties. Stronger external heavy atom effect (EHE)²³ has been observed in halogen-substituted *N*-alkylcarbazole by varying the linker length and thus the halogen-luminophore distance. However, the impact of ion separation on organic salts showing an unchanged ionic couple, to the best of our knowledge, has never been reported to date. Thus, the role of specific counterions requires immediate attention in order to develop a strategy to control the optical properties of charged luminophores. This will open new ways to design advanced purely organic room temperature phosphorescent (RTP) materials with tunable emissions by simply varying the counterions.

In this work we report on the preparation and characterization of a new class of ionic luminogens, namely benzimidazolium salts, **1**, with triflate, nitrate and iodide counterions featuring different sizes and electronic properties. Four crystal structures are isolated depending on the relative anion and crystallization solvent producing two diverse nitrate crystals which differ in their ionic distances. The resulting compounds exhibit multiple emissions in the solid-state, spanning from fluorescence (FL) to

^a Department of Chemistry, University of Milan and INSTM Research Unit, Via C. Golgi 19, 20133 Milan, Italy. E-mail: gabriele.dicarlo@unimi.it

^b CNR-SCITEC, Istituto di Scienze e Tecnologie Chimiche “G. Natta”, Via C. Golgi 19, 20133 Milan, Italy. E-mail: alessandra.forni@scitec.cnr.it

^c CNR-SCITEC, Istituto di Scienze e Tecnologie Chimiche “G. Natta”, Via A. Corti 12, 20133 Milano, Italy

† Electronic supplementary information (ESI) available. CCDC 2018732–2018735. For ESI and crystallographic data in CIF or other electronic format see DOI: 10.1039/d1tc00503k

molecular phosphorescence (PH_M) and supramolecular phosphorescence (PH_S). Both the distance and the nature of counterions are found to have an impact on the photophysical behavior by affecting both molecular and supramolecular features of **1**-salts. Spectroscopic studies along with theoretical investigations and structural analysis shed light on the role of ion-pairing, evidencing a three-fold impact on the emissive behavior of **1**-salts: FL quenching, PH_M enhancing and direct excitation triggering of triplet-states.

Results and discussion

Synthetic procedures

The synthetic procedures for the preparation of triflate (**1-OTf**), nitrate (**1-NO₃**) and iodide (**1-I**) salts of 1,3-dimethyl-2-(4-methylphenyl)-1*H*-benzimidazolium (**1**) salts are trivial and occur with excellent yields under mild conditions (Scheme 1).²⁴ *o*-Phenylenediamine and *p*-tolualdehyde in ethanol at room temperature undergo efficient (>90%) oxidative condensation (i) to give the benzimidazole core through hypervalent iodine generated *in situ* from $\text{Bu}_4\text{NI}/\text{H}_2\text{O}_2$. The following double alkylation of nitrogen atoms (ii) with iodomethane and *t*BuOK in THF at 60 °C results in benzimidazolium iodide, **1-I** in very good yield (>70%). **1-I** can be quantitatively reacted with appropriate silver salts through the metathesis reaction thus giving **1-OTf** and **1-NO₃**. The high purity grade of the final products, required for photophysical measurements, is obtained by flash chromatography through the automated Biotage[®] system and multiple recrystallizations with proper solvents.

Solutions

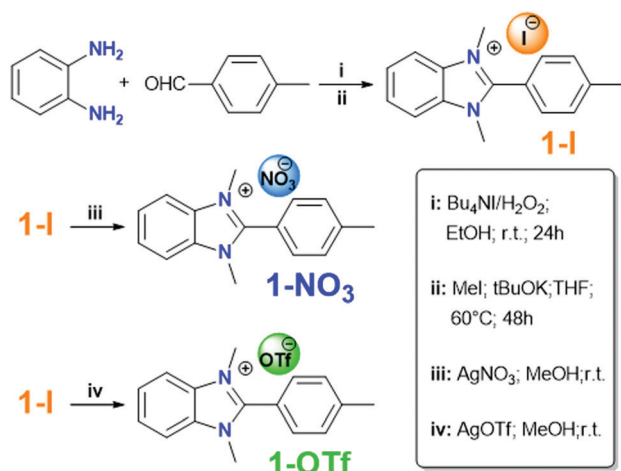
Absorption spectra of **1**-salts in a diluted solution of polar solvents (MeOH/EtOH 1:4) show three maxima at 210, 240 and 280 nm (Fig. S4a, ESI[†]). Similarly, the photoluminescence spectra (PL) at 298 K ($\lambda_{\text{exc}} = 300$ nm, see Table 1 and Fig. 1 left) show intense fluorescence at 345 nm (lifetime, τ , 1.54–1.57 ns) with a slight variation of quantum yields among the three salts

(Φ equal to 77.5, 52.6 and 53.6% for **1-OTf**, **1-NO₃** and **1-I** respectively). At 77 K (Fig. 1 right), alongside the FL, a very weak structured phosphorescence emerges at about 450 nm ($\tau_{\text{av}} > 2$ s, see Table 1 and Fig. S5, ESI[†]).

A combination of photophysical and NMR studies on diluted solutions of **1**-salts in a low polar solvent has been performed in order to study the ion pairing effect. NMR studies of the three salts confirm an effect of the counterion moving from polar DMSO- d_6 (Fig. S1, ESI[†]) to non-polar CDCl_3 solutions (Fig. S2, ESI[†]) as also reported for π -twisted benzimidazolium chromophores.²⁵ In DMSO- d_6 all the $^1\text{H-NMR}$ signals of the three salts are superimposable, while in CDCl_3 the chemical shifts of hydrogens, adjacent to the imidazolium ring ($\text{CH}_3\text{-N}$ and Hc), are affected by the nature of the counterion, in agreement with a tighter ion pairing in the solvent with a lower dielectric constant.^{26,27}

Likewise a bigger downfield shift of signals has also been reported for bromine-substituted *N*-alkylcarbazole as a result of the strongest interaction between the halogen and nitrogen atoms in derivatives with shortest linkers.²³ In **1**-salts, an increase in the electronegative character of counterions results in a higher net positive charge of nitrogen atoms shifting the protons to lower fields. This agrees with the more deshielded $\text{CH}_3\text{-N}$ and Hc protons of **1-I** compared to those of **1-NO₃** and **1-OTf**. To exclude any possible effect due to the low solubility of the salts in a non-polar solvent, their $^1\text{H-NMR}$ spectra have also been recorded in CDCl_3 at the same concentration (10^{-5} M) as used for photophysical studies (Fig. S2, ESI[†]). Under these conditions, $^1\text{H-NMR}$ spectra show the same deshielding trend as that displayed by more concentrated solutions (10^{-3} M). Very similar behavior was previously reported by some of us regarding the chemical shift of protons, in the α position to the positively charged nitrogen atom, of various methyl-pyridinium salts recorded in CDCl_3 .²⁸

The $^1\text{H-NMR}$ spectra of the three samples have also been obtained from CD_3OD solutions (Fig. S3, ESI[†]). The Hc and $\text{CH}_3\text{-N}$ signals of **1**-salts are affected by the specific ionic pair observed in CDCl_3 solutions (**1-I** > **1-NO₃** \geq **1-OTf**) although to a lesser extent. This could reasonably suggest that the counterion still plays a role in influencing the photophysical properties in alcoholic solution by explaining the slight variation in the recorded quantum yields of the investigated salts in MeOH/EtOH diluted solutions. Accordingly, the differences in the optical properties become more prominent when the three compounds are dissolved in CHCl_3 (10^{-5} M). The same absorption bands (240 and 282 nm) are observed for the three salts in polar and non-polar solvents (Fig. S4a and S4b respectively, ESI[†]), while the emissive properties are more significantly affected. A severe quenching of fluorescence intensities at 345 nm ($\Phi = 43.6, 3.4$ and 1.7% for **1-OTf**, **1-NO₃** and **1-I** respectively) is flanked by long-lived ($\tau_{\text{av}} = 4.34\text{--}5.58$ ms) components at 450 nm (Table 1 and Fig. S6, ESI[†]) which become visible in the steady-state PL spectra under direct triplet-excitation at 350 nm (Fig. S4c, ESI[†]). Direct population of triplet states has been recently reported as a feasible way to bypass $\text{S}_1\text{-T}_1$ ISC and improve the phosphorescence quantum efficiency²⁹ or as a means to visualize the



Scheme 1 Schematic synthetic procedure for the preparation of **1-I**, **1-NO₃** and **1-OTf**.

Table 1 Photophysical properties of **1**-salts at room temperature and 77 K

Entry	Solution		Entry	Solid state				
	MeOH/EtOH	CHCl ₃		Crystal	Powder			
1-OTf	Φ_{300} 77.5%	Φ_{300} 43.6%	1-OTf	Φ_{300} 50.7%	Φ_{350} 34.7%	Φ_{300} 57.9%	Φ_{350} 23.2%	
FL	345 nm 0.94 ns 1.54 ns ^a	345 nm 1.17 ns	FL	345 nm 0.89 ns 0.94 ns ^a				
PH_M	450 nm 2446.00 ms ^a	450 nm 4.59 ms	PH_M	410 nm 3.08 ms 46.80 ms ^a				
			PH_S	530 nm 327.33 ms 1096.10 ms ^a				
1-NO₃	Φ_{300} 52.6%	Φ_{300} 3.4%	1-NO₃-EtOH	Φ_{300} 3.7%	Φ_{350} 73%	Φ_{300} 2.2%	Φ_{350} 71%	
FL	345 nm 1.21 ns 1.57 ns ^a	345 nm 0.97 ns	FL	345 nm 0.65 ns 0.66 ns ^a				
PH_M	450 nm 2230.30 ms ^a	450 nm 5.85 ms	PH_M	415 nm 5.43 ms 29.26 ms ^a				
			PH_S	530 nm 8.23 ms 1104.40 ms ^a				
			1-NO₃-H₂O	Φ_{300} 1.9%	Φ_{350} 25%	Φ_{300} 4.0%	Φ_{350} 34.4%	
			FL	345 nm 0.42 ns 0.76 ns ^a				
			PH_M	415 nm 11.43 ms 35.31 ms ^a				
			PH_S	530 nm 12.18 ms 1178.50 ms ^a				
1-I	Φ_{300} 53.6%	Φ_{300} 1.7%	1-I-CH₂Cl₂	Φ_{300} 11.4%	Φ_{350} 23.7%	Φ_{300} 15.6%	Φ_{350} 26.1%	
FL	345 nm 1.20 ns 1.55 ns ^a	345 nm 1.05 ns	FL	345 nm 0.45 ns 1.05 ns ^a				
PH_M	450 nm 2232.60 ms ^a	450 nm 4.36 ms	PH_M	460 nm 6.15 ms 59.08 ms ^a				
			PH_S	530 nm 15.03 ms 1145.50 ms ^a				

^a Measurements conducted at 77 K. ^b PH_M not detectable (only τ in ns timescale attributed to the intense FL component).

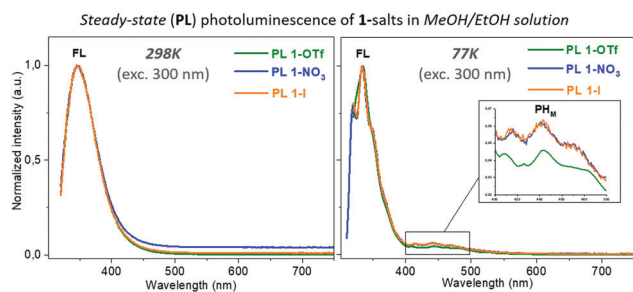


Fig. 1 Emission spectra (300 nm excitation wavelength) of diluted solutions (10^{-5} M in MeOH/EtOH) of **1-OTf** (green), **1-NO₃** (blue) and **1-I** (orange).

phosphorescent emission when overwhelmed by fluorescence.³⁰ Being visible also in polar solvents at 77 K, (Fig. 1, right side) such a high energy long-lived emission is ascribed to molecular origin (PH_M) as also corroborated by computational investigation (*vide infra*). Time-delayed spectra further show very weak phosphorescence emissions emerging over 500 nm (Fig. S4c, ESI[†]). As discussed in the section related to the solid-state, such a low-energy emission is attributed to supramolecular behavior (PH_S), associated with the possible formation of nanoaggregates in non-polar solution. The switching on of PH_M in CHCl₃ solutions at room temperature suggests an easier singlet–triplet (S–T) intersystem crossing (ISC) by ion-pairing assistance. The drop of

quantum efficiencies of **1**-salts in CHCl₃ suggests that the fluorescence quenching is strongly correlated with the closeness of the anion and its electronegative character (**I** > **NO₃** ≥ **OTf**). In agreement, the highest fluorescence quantum efficiency has been observed in **1-OTf**, which is endowed with the weakest ion-pairing in solutions. The theoretical study well elucidates the PL characteristics observed for **1**-salts in solution. The simulated TDDFT absorption spectrum of the isolated cation **1** displays three bands at 193, 220 and 245 nm (see Fig. S14 and Table S3 (ESI[†]) for the first singlet and triplet excitation energies). Its overall shape reproduces the experimental one collected in MeOH/EtOH (v/v 1/4) for the three salts (all displaying three absorptions at $\lambda_{\text{abs}} = 210, 240$ and 280 nm), though the computed maxima are shifted towards slightly higher energies. The S₀ → S₁ excitation (oscillator strength $f = 0.60$) is mainly (75%) a HOMO → LUMO transition where both HOMO and LUMO are π orbitals, delocalized over the whole molecule (Fig. S15, ESI[†]). Analysis of the first singlet and triplet states of **1** reveals the presence of a triplet level (T₂) of (π, π^*) character just below S₁ ($\Delta E = 0.162$ eV, 8 nm). Such a small S–T energy gap could allow an otherwise forbidden ISC from the singlet (S₁) to the close triplet state (T₂) which decays to T₁ by internal conversion. This explains the observed molecular phosphorescence (from T₁) accompanying the fluorescence (from S₁) of luminogen **1** in MeOH/EtOH solution at 77 K.

To explore the possible effect of the counterion on the electronic levels of **1**, calculations on the **1-OTf**, **1-NO₃** and **1-I** ionic pairs have also been carried out, starting from the respective X-ray structures of the three salts (see below) and freezing angles and torsions to preserve the relative arrangement of the ions as observed in the crystals (for **1-NO₃** the structure of **1-NO₃·H₂O** has been considered as the starting point). The first significantly populated (*i.e.* with $f > 0.1$) singlet excited state, despite its charge transfer (CT) character from the anion towards **1** (Fig. S16, ESI[†]), is only slightly shifted towards lower energies (248, 249 and 253 nm for **1-OTf**, **1-NO₃** and **1-I**, respectively, see Table S4, ESI[†]) than that computed for **1** (245 nm), in accordance with the nearly superimposable absorption spectra recorded in polar and non-polar solutions. Looking at the closest triplet levels, it is found that the S-T energy gap further reduces from 0.162 (**1**) to 0.068 (both **1-OTf** and **1-NO₃** pairs) and 0.010 eV (**1-I**), triggering an even easier S-T ISC with respect to the isolated cation in accordance with FL quenching and PH_M enhancement observed in non-polar solvent. Notably, the lowest S-T energy gap calculated for **1-I** agrees well with the strongest electronegative character of iodide as evidenced by ¹H-NMR analysis.

Solid state

In the solid state, **1**-salts exhibit concomitant fluorescence and multiple phosphorescence emissions whose relative position, intensity and lifetime at room temperature are strongly dependent on the counterion and crystal features.

Four different crystalline phases have been isolated from acetonitrile/H₂O (**1-NO₃·H₂O**), ethanol (**1-OTf** and **1-NO₃·0.5EtOH**) and dichloromethane (**1-I·0.5CH₂Cl₂**). By exciting all crystals at 300 nm at room temperature, fluorescence (τ in the ns regime, see Table 1 and Fig. S7–S11, ESI[†]) emission at about 350 nm is observed together with phosphorescent components with properties depending on the specific anion and its relative distance from the cation (see Table 1, Fig. 2 and Fig. S7a, ESI[†]). In particular, while the steady-state spectrum of **1-OTf** (Fig. 2a, solid-line) displays only an intense fluorescent emission (FL), the time-delayed spectrum (Fig. 2a, dotted-line) reveals the presence of two phosphorescences at 410 nm ($\tau_{av} = 23.08$ ms, PH_M) and 530 nm ($\tau_{av} = 327.33$ ms, PH_S). Interestingly, for crystals of **1-NO₃·H₂O** and **1-NO₃·0.5EtOH** the PH_M component (at 415 nm, $\tau_{av} = 11.43$ and 5.43 ms, respectively) is already observed in the steady-state spectrum together with FL at 350 nm (see Fig. 2a and Fig. S7a, ESI[†]). An additional long-lived component PH_S can be detected at 530 nm ($\tau_{av} = 12.18$ and 8.23 ms for **1-NO₃·H₂O** and **1-NO₃·0.5EtOH**, respectively) in the time-delayed spectra. The PL spectrum of **1-I·0.5CH₂Cl₂** displays an almost undetectable FL and an intense, broad phosphorescence band PH_M at 460 nm ($\tau_{av} = 6.15$ ms). Again, PH_S is detected only in the delayed spectrum at 530 nm ($\tau_{av} = 15.03$ ms). It is worth noting that the red shift of the PH_M band observed in nitrate (5 nm) and iodide (50 nm) salts with respect to that of triflate, follows the trend of the electronegative character of the anions.

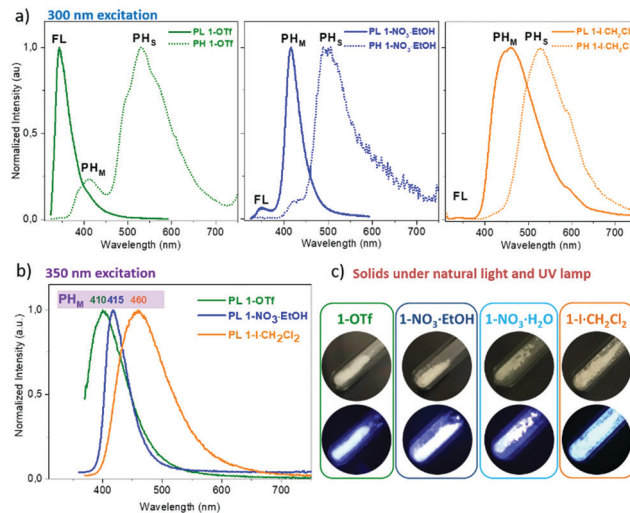


Fig. 2 (a) Steady state (solid line) and time-delayed (dotted line) photoluminescence emission at 300 nm excitation wavelength; (b) steady-state photoluminescence emission at 350 nm excitation wavelength; and (c) photographs of **1**-salt powders under natural and UV light (366 nm).

To disclose the effect of counterions on solid state photo-physical properties, the crystal structures of the four salts have been determined by single crystal X-ray diffraction analysis. **1-OTf**, **1-NO₃** and **1-I** crystallize in the $P\bar{1}$ (**1-OTf** and **1-NO₃·H₂O**) and $C2/c$ (**1-NO₃·0.5EtOH** and **1-I·0.5CH₂Cl₂**) space groups (see Fig. 3 and Fig. S12, ESI[†]). The asymmetric units of **1-NO₃·H₂O** and **1-I·0.5CH₂Cl₂** include one water and one-half dichloromethane cocrystallized molecule, respectively, while that of **1-NO₃·0.5EtOH** comprises three independent ionic pairs (labelled as A, B and C) and one and a half ethanol cocrystallized molecule. XRD analysis shows that **1** is far from being planar, as indicated by the dihedral angle between the least-squares (l.s.) planes through the benzimidazole moiety and the phenyl ring, varying in the range 48.23–52.35° in the four structures.

The benzimidazole moiety forms in all cases stacks of head-to-tail π - π dimeric aggregates. Two independent stacks are found in the crystal structure of **1-NO₃·0.5EtOH**, one built up of A molecules and the other from B and C molecules. Along the stacks, the distances between benzimidazole centroids are alternately equal to 3.610 and 4.316 Å (**1-OTf**), 3.555 and

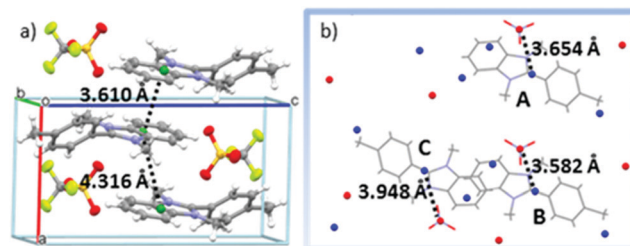


Fig. 3 Fragment of crystal packing of (a) **1-OTf** with shortest distances between benzimidazole centroids (green circles) and (b) **1-NO₃·0.5EtOH** with shortest distances between the cation and anion (blue and red circles, respectively) centroids for three independent ionic pairs.

4.526 Å (**1-NO₃·H₂O**), 3.416/3.487 and 5.227/5.180 Å (**1-NO₃·0.5EtOH**, stacks A/B,C) and 3.566 and 4.767 Å (**1-I·0.5CH₂Cl₂**). The short distances between centroids suggest the presence of H-dimers owing to very little slippages (0.49, 0.46, 0.53 and 0.62 Å for **1-OTf**, **1-NO₃·H₂O**, **1-NO₃·0.5EtOH** and **1-I·0.5CH₂Cl₂**, respectively, considering, for **1-NO₃·0.5EtOH**, the H-dimer of A molecules) and the values of the angle θ between the centroid-centroid vector and its projection on the molecular plane (82, 83, 81 and 80° in the same order as above). Such H-dimers are laterally shifted along the stacks with much larger slippages (2.3, 2.8, 4.0 and 3.1 Å and $\theta = 58, 52, 40$ and 49° for **1-OTf**, **1-NO₃·H₂O**, **1-NO₃·0.5EtOH** and **1-I·0.5CH₂Cl₂**, respectively). In all structures, the cations are laterally connected *via* CF₃SO₃⁻ or NO₃⁻ or I⁻ anions through weak C-H...X (X = F, O in triflate; X = N, O in nitrates and X = I in iodide) hydrogen bonds (HB). The strongest interactions correspond to H...X distances/C-H...X angles of 2.45 Å/169° (X = O, **1-OTf**), 2.49 Å/177° (X = O, **1-NO₃·H₂O**), 2.36 Å/162° (X = O, **1-NO₃·0.5EtOH**) and 2.91 Å/170° (X = I, **1-I·0.5CH₂Cl₂**). In addition, in both nitrate structures the cocrystallized solvent molecules behave as HB donors of medium strength with oxygen atoms of NO₃⁻ anions. The CH₂Cl₂ cocrystallized molecule in **1-I**, on the other hand, is weakly hydrogen bonded to both **1** and I⁻, in agreement with a slow loss of crystallinity at room temperature.

The separations between ionic pairs in the four structures (see Fig. 3b for **1-NO₃·0.5EtOH** and Fig. S13, ESI[†]) reveal that the shorter distances between cation-anion centroids increase from 3.582 to 4.385, 4.596 and 5.296 Å moving from **1-NO₃·0.5EtOH** to **1-I·0.5CH₂Cl₂**, **1-NO₃·H₂O** and **1-OTf**, respectively. This trend clearly does not reproduce that expected from NMR investigation, according to which the cation-anion distances should increase in the order **I** < **NO₃** ≤ **OTf** based only on the electronegativity effect. In the crystal state other factors come into play and result in the shortest value for **1-NO₃·0.5EtOH**. This is obviously imputable to the reduced dimensions of the counter-ion (compared to that of **1-OTf**) and of the cocrystallized solvent molecule (compared to that of **1-I·0.5CH₂Cl₂**) and to the 2 : 1 ratio between the ionic pair and cocrystallized solvent molecule (compared to the 1 : 1 ratio in **1-NO₃·H₂O**). Thus, the strength of the ionic pair concomitantly depends on the anion electronegativity and cation-anion distances and is expected to be reduced from the most electronegative iodide to the less electronegative and more distant triflate. However, the close proximity of nitrate to the cation could reasonably provide a reinforced ion-pairing in **1-NO₃·0.5EtOH**.

These analyses, together with theoretical calculations reported above, allow justifying the photophysical behavior of crystalline **1**-salts. The presence of heavy atoms along with the narrowest S-T gap computed for **1-I·0.5CH₂Cl₂** well agree with an easier ISC, thus producing PH_M enhancement and concomitant FL quenching as a result of the strong EHE. On the other hand, the **1-OTf** PL-spectrum shows only the FL band while in **1-NO₃** both FL and PH_M are displayed. Noticeably, the emissive patterns of **1-NO₃·0.5EtOH** and **1-NO₃·H₂O** salts, equipped with the same counterion but with different anion-cation center of mass separation, show the inverted ratio of FL and PH_M

intensities (Fig. S7a, ESI[†]). **1-NO₃·H₂O** displays intense FL and weak PH_M while **1-NO₃·0.5EtOH** displays the opposite, confirming that the ion-pairing effect increases with reducing distances between the ions thus making the ISC easier. Accordingly, by decreasing the ionic distance, fluorescence is quenched and the intensity of phosphorescence increase. Although the co-crystallized solvent effect cannot be totally excluded, the impact of ionic distance on photophysical properties of the same ionic couple has never been investigated to date.

As expected by a reinforced ion-pairing, the decrease in the fluorescence quantum efficiency in crystalline **1-OTf**, **1-NO₃·0.5EtOH**, **1-NO₃·H₂O** and **1-I·0.5CH₂Cl₂** follows a trend similar to that observed in CHCl₃ solutions (Φ equal to 51, 4, 2 and 11%, respectively). The weak cation-anion interaction in **1-OTf** produces the highest quantum efficiency observed at 300 nm excitation and guarantees ultrabright FL emission both in the solution and in solid state.

Concerning the low energy phosphorescence, PH_S, of the four salts, the single crystal XRD study allows explaining that its origin is due to the presence of H-dimers in their crystal structure, as thoroughly demonstrated for other luminophores.^{11,31}

The presence of cocrystallized solvent, as well, may play a role in the observed solid-state behavior introducing non radiative deactivation paths. In fact, shorter lifetimes are measured for **1-NO₃·H₂O** (12.18 ms), **1-NO₃·0.5EtOH** (8.23 ms) and **1-I·0.5CH₂Cl₂** (15.03 ms) crystals compared with that of the solvent free **1-OTf** salt (327.33 ms) which exhibits ultralong RTP with an afterglow of up to 2s. The different lifetimes of the two phosphorescence emissions at room temperature allow observing the blue to green color variation with the naked eye (Fig. 4).

In agreement with the excitation spectra (Fig. S7, ESI[†]), the T₁ state of the four crystals can be directly populated by exciting at 350 nm. As stated above, the direct excitation of triplet-states allows visualizing the PH_M emission overwhelmed by intense FL.³⁰ The corresponding PL emission spectrum of **1-OTf** crystals (Fig. 2b), in fact, shows only PH_M at 410 nm ($\Phi_{350} = 34.7\%$). Similarly, the PL spectra of nitrate and iodide crystals exhibit their corresponding PH_M bands (Fig. 2b) with a sizable enhancement of quantum efficiencies. Remarkably, **1-NO₃·0.5EtOH** crystals show impressively high phosphorescence quantum efficiency ($\Phi_{350} = 73\%$).^{15,32} **1-NO₃·H₂O** and **1-I·0.5CH₂Cl₂** crystals exhibit a minor, still consistent, increase in their relative quantum yields ($\Phi_{350} = 25\%$ and 23.7% respectively). Such an efficient direct population of the triplet state, reflecting in quantum yields above 20% in all crystals, is

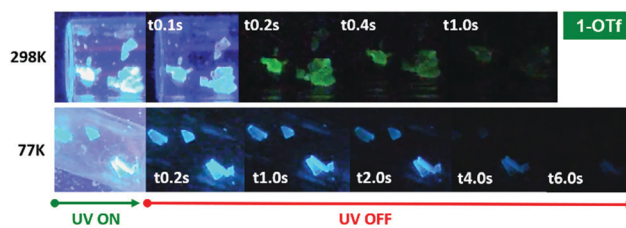


Fig. 4 Afterglow of **1-OTf** crystals at 298 K and 77 K before and after ceasing UV excitation (366 nm).

also evidenced by their bright luminescence under the excitation of a 366 nm lamp (Fig. 2c). Except for **1-OTf**, which shows a lowering in the quantum efficiency when moving from 300 to 350 nm excitation wavelengths, most likely attributed to the loss of the intense FL emission, a boosted quantum yield is observed for **1-NO₃·0.5EtOH**, **1-NO₃·H₂O** and **1-I·0.5CH₂Cl₂** crystals. In agreement, these latter ones show, at 350 nm excitation, higher ratios between radiative (K_r) and non-radiative rate constant (K_{nr}) than those obtained by exciting at 300 nm (Table S1, ESI[†]).

Despite the presence of solvent molecules in the crystal packing, the direct triplet-excitation of **1-NO₃·0.5EtOH** crystals produces the highest phosphorescence quantum efficiency in the series. Considering the same counterion in **1-NO₃·0.5EtOH** and **1-NO₃·H₂O**, the former is characterized by the shorter distance between cation–anion centers of mass (3.582 vs. 4.596 Å), and smaller non-radiative ($K_{nr} = 50.00$ vs. 65.56 s⁻¹) and greater radiative ($K_r = 135.19$ vs. 21.85 s⁻¹) rate constants. Once again this supports the role played by the counterion and its vicinity to the luminophore in activating the phosphorescence emission. Furthermore, the differences in quantum efficiencies observed between the two nitrate salts under 350 nm excitation suggest that the stronger the ion-pairing, the more efficient the direct triplet-excitation.

Crystallinity dependent optical responses

The multi-emissive patterns of **1**-salts vary with mechanical stimuli produced by the grinding of crystalline samples in an agate mortar. By excitation at 300 nm, ground **1-I** and **1-NO₃** (both forms) exhibit FL enhancement and PH_M quenching (Fig. 5) but almost unchanged overall quantum efficiency. Ground **1-OTf** displays a slight increase only in its fluorescent emission ($QY_{300} = 57.9\%$).

Upon excitation at 350 nm, the effect of grinding on the isolated phosphorescence emission can be analyzed. Ground **1-OTf** shows a reduced QY_{350} (23.2%) with respect to that obtained in highly ordered crystals (34.7%). On the other hand, in **1-NO₃·0.5EtOH**, the variation of QY_{350} is almost negligible after mechanical micronization. Finally, an increased QY_{350} is observed for both ground **1-NO₃·H₂O** ($\Phi_{350} = 34.4\%$) and **1-I·0.5CH₂Cl₂** ($\Phi_{350} = 26.1\%$). Such variations could be ascribed to a number of factors including, for example, the partial loss of the loosely packed cocrystallized solvent, the introduction of

surface defects and the reduction of crystal sizes,^{33–35} all of them affecting the photophysical properties of ground **1**-salts.

Conclusions

In this work, we develop a facile strategy to manipulate the emissive properties of a new class of ionic luminogens, prepared with different counterions, *i.e.* triflate, iodide and nitrate, based on benzimidazolium ion **1**. The photophysical study along with theoretical calculations, single crystal X-ray diffraction analysis and ¹H-NMR investigation, performed in diluted solutions of both polar and low polar solvents, have allowed disclosing the effect of the counterion on molecular and supramolecular emissive properties of **1**-salts. Four crystals have been obtained, *i.e.*, **1-OTf**, **1-I·0.5CH₂Cl₂**, **1-NO₃·H₂O** and **1-NO₃·0.5EtOH**. They display at room temperature multiple emissions, comprising fluorescence (FL), molecular phosphorescence (PH_M) and supramolecular phosphorescence (PH_S), the latter associated with the presence of strong π - π stacking interactions in the crystal structures. The position and relative intensities of these emissions are found to depend on the nature of the counterion as a combination of ion-pairing effects and supramolecular interactions. In particular, crystals of **1-OTf**, displaying a weaker anion–cation interaction, provide ultrabright fluorescence and supramolecular long-lasting RTP; **1-I·0.5CH₂Cl₂** crystals mainly show molecular phosphorescence, promoted by the EHE of iodide counter-ion granting an efficient singlet–triplet ISC; nitrate salts, characterized by different cation–anion distances, exhibit simultaneous fluorescence and molecular phosphorescence. More specifically, crystals of **1-NO₃·H₂O** display intense FL and weak PH_M while those of **1-NO₃·0.5EtOH** show an opposite trend. For the latter salt, having the shortest anion–cation distance within the series of examined compounds, an impressive phosphorescence quantum efficiency is obtained by the direct population of the triplet states.

These findings clearly demonstrate that strong ion-pairing is associated with (i) severe quenching of fluorescence; (ii) enhancement of molecular phosphorescence by facilitating singlet–triplet ISC; (iii) efficient direct population of triplet states. The supramolecular long-lasting RTP observed at lower energies appears to be less affected by the specific anion owing to the close similarity in the stacking pattern of the examined structures. The presence of co-crystallized solvent molecules, however, clearly affects the PH_S lifetimes, which are significantly longer for **1-OTf**, free from co-crystallized solvent molecules, than for the other salts.

The results obtained for the ion-pairing effects are expected to contribute to the understanding of the key-principles governing the emissive properties of ionic salts, providing a tool for the design of new luminescent ionic molecules with fine-tailored optical properties.

Author contributions

G. D. C. and P. M. synthesized and characterized **1**-salts. D. M. performed the photophysical study. C. B. performed time-delayed

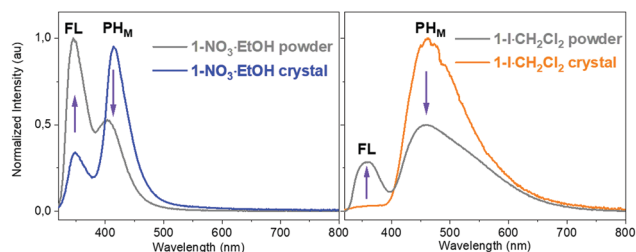


Fig. 5 PL spectra of **1-NO₃·0.5EtOH** and **1-I·0.5CH₂Cl₂** solids before (blue and orange lines respectively) and after grinding (grey lines) ($\lambda_{exc} = 300$ nm).

spectroscopic investigation. A. F. performed crystallography and computational investigation. F. T. recorded the absorption spectra and performed data curation and M. P. was involved in editing processes. The project was conceived by E. C., A. F. and G. D. C. The manuscript was written by E. C., A. F. and G. D. C. All authors have given approval to the final version of the manuscript.

Conflicts of interest

There are no conflicts to declare.

Acknowledgements

The use of instrumentation purchased through the Regione Lombardia-Fondazione Cariplo joint SmartMatLab Project is gratefully acknowledged. G. D. C. greatly thanks the University of Milan (Piano Sostegno alla Ricerca 2018 LINEA 2 Azione A – Giovani Ricercatori) for financial support.

References

- 1 S. Hirata, *Adv. Opt. Mater.*, 2017, **5**, 1700116.
- 2 S. Xu, Y. Duan and B. Liu, *Adv. Mater.*, 2020, **32**, 1903530.
- 3 F. Würthner, *Angew. Chem., Int. Ed.*, 2020, **59**, 14192–14196.
- 4 C.-R. Wang, Y.-Y. Gong, W.-Z. Yuan and Y.-M. Zhang, *Chin. Chem. Lett.*, 2016, **27**, 1184–1192.
- 5 A. Forni, E. Lucenti, C. Botta and E. Cariati, *J. Mater. Chem. C*, 2018, **6**, 4603–4626.
- 6 Kenry, C. Chen and B. Liu, *Nat. Commun.*, 2019, **10**, 2111.
- 7 E. Lucenti, A. Forni, C. Botta, L. Carlucci, C. Giannini, D. Marinotto, A. Pavanello, A. Previtali, S. Righetto and E. Cariati, *Angew. Chem., Int. Ed.*, 2017, **56**, 16302–16307.
- 8 W. Zhao, Z. He, J. W. Y. Lam, Q. Peng, H. Ma, Z. Shuai, G. Bai, J. Hao and B. Z. Tang, *Chem*, 2016, **1**, 592–602.
- 9 P. Alam, N. L. C. Leung, J. Liu, T. S. Cheung, X. Zhang, Z. He, R. T. K. Kwok, J. W. Y. Lam, H. H. Y. Sung, I. D. Williams, C. C. S. Chan, K. S. Wong, Q. Peng and B. Z. Tang, *Adv. Mater.*, 2020, **32**, 2001026.
- 10 Z. An, C. Zheng, Y. Tao, R. Chen, H. Shi, T. Chen, Z. Wang, H. Li, R. Deng, X. Liu and W. Huang, *Nat. Mater.*, 2015, **14**, 685–690.
- 11 E. Lucenti, A. Forni, C. Botta, L. Carlucci, C. Giannini, D. Marinotto, A. Previtali, S. Righetto and E. Cariati, *J. Phys. Chem. Lett.*, 2017, **8**, 1894–1898.
- 12 S. d'Agostino, F. Spinelli, P. Taddei, B. Ventura and F. Grepioni, *Cryst. Growth Des.*, 2019, **19**, 336–346.
- 13 A. S. Carretero, A. S. Castillo and A. F. Gutiérrez, *Crit. Rev. Anal. Chem.*, 2005, **35**, 3–14.
- 14 H. Shi, Z. An, P.-Z. Li, J. Yin, G. Xing, T. He, H. Chen, J. Wang, H. Sun, W. Huang and Y. Zhao, *Cryst. Growth Des.*, 2016, **16**, 808–813.
- 15 G. Chen, S. Guo, H. Feng and Z. Qian, *J. Mater. Chem. C*, 2019, **7**, 14535–14542.
- 16 Y. Li, Y. Lei, L. Dong, L. Zhang, J. Zhi, J. Shi, B. Tong and Y. Dong, *Chem. – Eur. J.*, 2019, **25**, 573–581.
- 17 W. Xi, J. Yu, M. Wei, Q. Qiu, P. Xu, Z. Qian and H. Feng, *Chem. – Eur. J.*, 2020, **26**, 3733–3737.
- 18 Z. Cheng, H. Shi, H. Ma, L. Bian, Q. Wu, L. Gu, S. Cai, X. Wang, W. Xiong, Z. An and W. Huang, *Angew. Chem., Int. Ed.*, 2018, **57**, 678–682.
- 19 J. Wang, X. Gu, H. Ma, Q. Peng, X. Huang, X. Zheng, S. H. P. Sung, G. Shan, J. W. Y. Lam, Z. Shuai and B. Z. Tang, *Nat. Commun.*, 2018, **9**, 2963.
- 20 G. Chen, H. Feng, F. Feng, P. Xu, J. Xu, S. Pan and Z. Qian, *J. Phys. Chem. Lett.*, 2018, **9**, 6305–6311.
- 21 G. Zhang, X. Zhang, L. Kong, S. Wang, Y. Tian, X. Tao and J. Yang, *Sci. Rep.*, 2016, **6**, 37609.
- 22 J. Wang, X. Gu, P. Zhang, X. Huang, X. Zheng, M. Chen, H. Feng, R. T. K. Kwok, J. W. Y. Lam and B. Z. Tang, *J. Am. Chem. Soc.*, 2017, **139**, 16974–16979.
- 23 X. Sun, B. Zhang, X. Li, C. O. Trindle and G. Zhang, *J. Phys. Chem. A*, 2016, **120**, 5791–5797.
- 24 S. Riera-Galindo, A. Orbelli Biroli, A. Forni, Y. Puttisong, F. Tessore, M. Pizzotti, E. Pavlopoulou, E. Solano, S. Wang, G. Wang, T.-P. Ruoko, W. M. Chen, M. Kemerink, M. Berggren, G. di Carlo and S. Fabiano, *ACS Appl. Mater. Interfaces*, 2019, **11**, 37981–37990.
- 25 A. J.-T. Lou, S. Righetto, E. Cariati and T. J. Marks, *Chem. – Eur. J.*, 2018, **24**, 15801–15805.
- 26 F. Tessore, D. Roberto, R. Ugo, P. Mussini, S. Quici, I. Ledoux-Rak and J. Zyss, *Angew. Chem., Int. Ed.*, 2003, **42**, 456–459.
- 27 F. Tessore, D. Locatelli, S. Righetto, D. Roberto, R. Ugo and P. Mussini, *Inorg. Chem.*, 2005, **44**, 2437–2442.
- 28 F. Tessore, E. Cariati, F. Cariati, D. Roberto, R. Ugo, P. Mussini, C. Zuccaccia and A. Macchioni, *ChemPhysChem*, 2010, **11**, 495–507.
- 29 J. Yuan, R. Chen, X. Tang, Y. Tao, S. Xu, L. Jin, C. Chen, X. Zhou, C. Zheng and W. Huang, *Chem. Sci.*, 2019, **10**, 5031–5038.
- 30 E. Lucenti, A. Forni, A. Previtali, D. Marinotto, D. Malpicci, S. Righetto, C. Giannini, T. Virgili, P. Kabacinski, L. Ganzer, U. Giovanella, C. Botta and E. Cariati, *Chem. Sci.*, 2020, **11**, 7599–7608.
- 31 A. Previtali, E. Lucenti, A. Forni, L. Mauri, C. Botta, C. Giannini, D. Malpicci, D. Marinotto, S. Righetto and E. Cariati, *Molecules*, 2019, **24**, 2552.
- 32 A. Fermi, G. Bergamini, R. Peresutti, E. Marchi, M. Roy, P. Ceroni and M. Gingras, *Dyes Pigm.*, 2014, **110**, 113–122.
- 33 A. Patra, N. Hebalkar, B. Sreedhar, M. Sarkar, A. Samanta and T. P. Radhakrishnan, *Small*, 2006, **2**, 650–659.
- 34 T. Han, Y. Hong, N. Xie, S. Chen, N. Zhao, E. Zhao, J. W. Y. Lam, H. H. Y. Sung, Y. Dong, B. Tong and B. Z. Tang, *J. Mater. Chem. C*, 2013, **1**, 7314–7320.
- 35 C. Botta, S. Benedini, L. Carlucci, A. Forni, D. Marinotto, A. Nitti, D. Pasini, S. Righetto and E. Cariati, *J. Mater. Chem. C*, 2016, **4**, 2979–2989.